



Measurement of angular distributions of  $\Upsilon(nS) \rightarrow \mu^+\mu^-$  decays  
in  $p\bar{p}$  collisions at  $\sqrt{s} = 1.96$  TeV

The CDF Collaboration  
URL <http://www-cdf.fnal.gov>  
(Dated: October 2, 2011)

The angular distributions of  $\Upsilon(nS) \rightarrow \mu^+\mu^-$  decays are analyzed using a sample of  $\Upsilon(1S)$ ,  $\Upsilon(2S)$  and  $\Upsilon(3S)$  mesons produced in  $p\bar{p}$  collisions at  $\sqrt{s} = 1.96$  TeV. The data sample used in this analysis was collected with the CDF II detector at the Fermilab Tevatron and corresponds to an integrated luminosity of  $6.7 \text{ fb}^{-1}$ . The angular distributions are analyzed as functions of the transverse momentum of the  $\mu^+\mu^-$  final state in both the Collins-Soper and the S-channel helicity frames. Consistency of the analysis is checked by comparing frame-invariant quantities derived from parametrizations of the angular distributions measured in each choice of reference frame. This analysis is the first to quantify the complete three-dimensional angular distribution of  $\Upsilon(1S)$ ,  $\Upsilon(2S)$  and  $\Upsilon(3S)$  decays and finds that their decays are nearly isotropic, even when produced with large transverse momentum.

## I. INTRODUCTION

Although the  $\mu^+\mu^-$  final state has been studied at hadron colliders for over four decades, the production of heavy quarkonia has proved to be difficult to describe accurately using models based on QCD. Models that accommodate the surprisingly large  $J/\psi$  and  $\Upsilon$  production cross sections[1, 2] also make specific predictions about their production polarization but these are generally in poor agreement with experimental measurements. Discrepancies between results obtained by different experiments[3, 4] suggest that quarkonia might be strongly polarized when produced, but that different experimental acceptances limit the ability to formulate a complete picture.

In fact, although the angular distributions of muons from  $\Upsilon \rightarrow \mu^+\mu^-$  decays can be written

$$\frac{d\Gamma}{d\Omega} \sim 1 + \lambda_\theta \cos^2 \theta + \lambda_\varphi \sin^2 \theta \cos 2\varphi + \lambda_{\theta\varphi} \sin 2\theta \cos \varphi \quad (1)$$

in the  $\Upsilon$  rest frame, previous experiments have only measured the  $\lambda_\theta$  parameter as a function of the  $\Upsilon$  transverse momentum. Since these measurements have only been carried out in the S-channel helicity frame, in which the  $z$ -axis is aligned with the  $\Upsilon$  momentum vector, it is possible that significant polarization could be present and would manifest itself by large values of  $\lambda_\varphi$  or  $\lambda_{\theta\varphi}$ , even when  $\lambda_\theta \sim 0$ .

The analysis described here is a new technique with which to study the angular distribution of muons in  $\Upsilon$  decay and is the first to provide information on all three coefficients, measured in multiple reference frames and to provide new tests that demonstrate a level of self-consistency.

## II. ANALYSIS OVERVIEW

Using a sample of events collected with di-muon triggers, we reconstruct oppositely charged muons and analyze those events which have invariant mass in the range  $8.3 < m(\mu^+\mu^-) < 11.7 \text{ GeV}/c^2$ . This event sample, obtained from  $6.7 \text{ fb}^{-1}$  of  $p\bar{p}$  collisions at  $\sqrt{s} = 1.96 \text{ GeV}$ , contains 550,000  $\Upsilon(1S)$ , 150,000  $\Upsilon(2S)$  and 76,000  $\Upsilon(3S)$  decays. The properties of di-muon candidates that have invariant mass near the  $\Upsilon(nS)$  resonances are described using a two-component model for the  $\Upsilon(nS)$  signal itself, and the background. The angular distribution of the  $\Upsilon(nS)$  component is extracted from the inclusive sample by means of constraints on the amount of background present in the sample and the angular distribution present in the background component. We find that the background is dominated by muons from  $b$ -decays and can be isolated by requiring that one muon is displaced, that is, it has an impact parameter inconsistent with production at the primary vertex. We verify that this sample has the same angular distribution as the complimentary prompt sample by comparing their angular distributions in mass regions that do not contain  $\Upsilon$  decays.

Furthermore, we observe that the shape of the background component of the di-muon invariant mass distribution is independent of whether a displaced muon is identified. Therefore, we constrain the amount of background in the prompt component by scaling the background distribution observed in the displaced component by a linear function of mass which is constrained by a simultaneous fit to the displaced sample and the mass sidebands of the prompt sample. With the amount of background under the  $\Upsilon(nS)$  signals constrained by the displaced sample and the scale factor, we perform a simultaneous fit to the two samples to determine the angular distribution in the background and in the  $\Upsilon(nS)$  decay component. This procedure preferable to extracting the angular distribution of the background from sidebands because we find evidence that the properties of muons produced in correlated  $b\bar{b}$  production evolves rapidly with invariant mass and transverse momentum.

## III. EVENT SELECTION

The CDF detector, which is described in detail elsewhere [5], uses several muon detection subsystems to identify muons for use in the Level 1 and 2 triggers and for subsequent reconstruction of the recorded events. The first muon detector, referred to as CMU consists of four layers of drift tubes that are located outside the hadron calorimeter and cover the central range of pseudo-rapidity  $|\eta| < 0.6$ . Additional layers of drift tubes and scintillator comprise the CMP muon system, which is located behind the magnetic flux return yoke, roughly covers the region  $|\eta| < 0.4$ . Muon detection in the region between  $0.6 < |\eta| < 1$  is provided by the CMX muon system, which is also constructed from scintillator and two layers of drift tubes. Tracking of charged particles is provided by a cylindrical drift chamber and five layers of double-sided silicon strip detectors.

We collect a sample of events using two triggers, both of which require the presence of a muon with  $p_T > 4 \text{ GeV}/c$  identified in the CMU and CMP systems (CMUP) in coincidence with a muon of opposite charge with  $p_T > 3 \text{ GeV}/c$

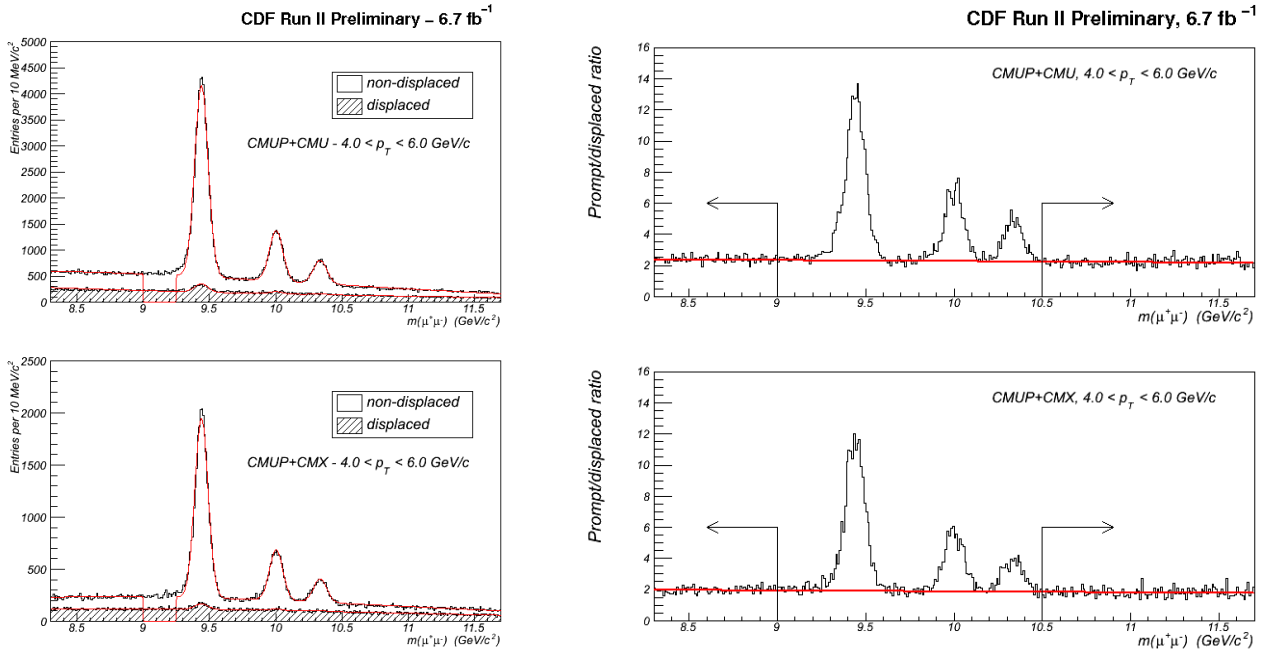


FIG. 1: Examples of invariant mass distributions of di-muon events triggered and reconstructed in CMUP+CMU (top) and in CMUP+CMX (bottom). The left figures show the prompt and displaced components separately while the right plots show their ratio. A small region of invariant mass below the  $\Upsilon(1S)$  is removed from the fit to the prompt sample to reduce sensitivity to the modeling of final state radiation. The arrows in the plots on the right indicate the regions of invariant mass in the prompt sample used to constrain the parameters in the prompt scale factor function.

identified in either the CMU or the CMX muon systems. Both muons are required to be identified after full event reconstruction and to satisfy criteria that test the quality of the match between the extrapolated track trajectory and the activity observed in the muon chambers. The Level 1 trigger efficiencies are measured using the unbiased muon in a sample of  $J/\psi \rightarrow \mu^+\mu^-$  decays collected with a single-muon trigger[6]. The Level 2 CMP trigger efficiency is measured using a sample of  $J/\psi \rightarrow \mu^+\mu^-$  decays triggered using only the CMU and CMX muon sub-systems.

#### IV. ANGULAR DISTRIBUTION ANALYSIS

The sample of events is analyzed separately in 8 ranges of di-muon transverse momentum. Within each range of  $p_T$ , events in the sample are classified as *displaced* if one of the muons has hits in at least three layers of the silicon detector and has an impact parameter, measured with respect to the average beam axis, of at least  $150 \mu\text{m}$ . The complementary sample is referred to as the *prompt* component. Figure 1 shows an example of the invariant mass distributions for muons in the prompt and displaced samples recorded with the CMUP+CMU and CMUP+CMX triggers. Only a small fraction (1-4%) of the  $\Upsilon$  signal is present in the displaced sample which is measured using a simultaneous fit to the prompt and displaced di-muon invariant mass distributions. The displaced sample and the subset of the prompt sample which has invariant mass below the  $\Upsilon(1S)$  and above the  $\Upsilon(3S)$  is fit to obtain a parametrization their ratio. A linear function describes the ratio well, but a quadratic function is also considered to quantify the sensitivity of the measured angular distributions to the assumed shape of the scale factor.

The events are analyzed in 12 separate ranges of invariant mass: three that isolate the  $\Upsilon(1S)$ ,  $\Upsilon(2S)$  and  $\Upsilon(3S)$  signals, and the rest containing primarily background. Within each range the decay angles of the positive muons are calculated in either the S-channel helicity frame or the Collins-Soper frame and their distributions are collected in  $20 \times 36$  bins of  $(\cos\theta, \varphi)$ . The number of events observed in each bin is proportional to the product of the detector acceptance,  $\mathcal{A}$ , and the underlying angular distribution,

$$\frac{dN}{d\Omega} \propto \mathcal{A}(\cos\theta, \varphi) \cdot w(\cos\theta, \varphi; \vec{\lambda}) \quad (2)$$

where  $w(\cos\theta, \varphi; \vec{\lambda})$  depends on parameters  $\vec{\lambda}$  that are adjusted to maximize a likelihood function that assumes Poisson distributed entries in each bin.

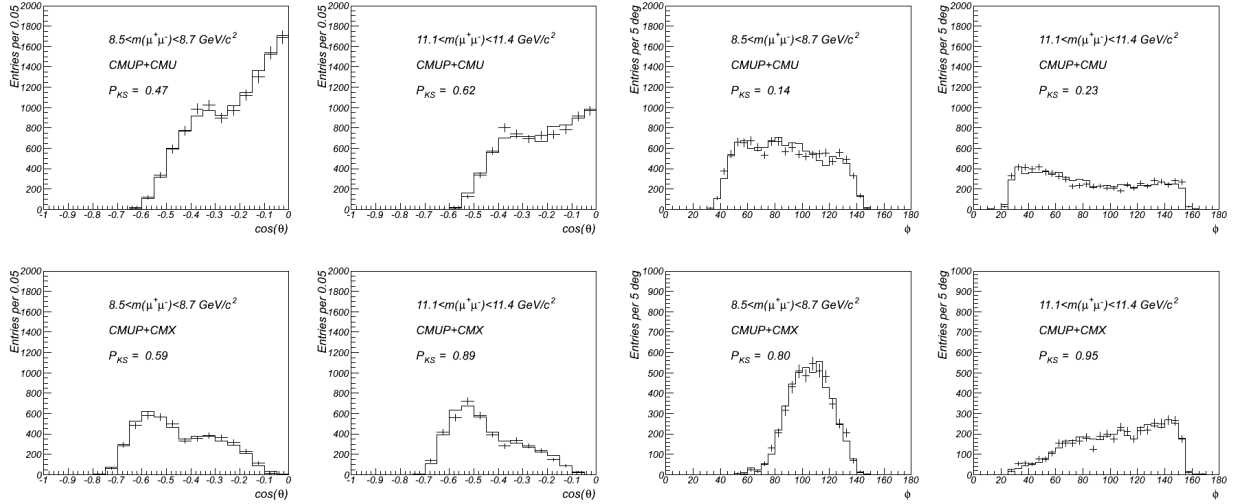
CDF Run II Preliminary, 6.7 fb<sup>-1</sup>

FIG. 2: Projections of angular distributions of prompt (histogram) and displaced samples (error bars) in two regions of invariant mass, one below the  $\Upsilon(1S)$  and one above the  $\Upsilon(3S)$  mass. The agreement is quantified using the Kolmogorov-Smirnov P-value,  $P_{KS}$ , indicated with each distribution.

The detector acceptance depends on both the geometric coverage of the muon and tracking detectors and on the kinematic requirements imposed by the trigger and event reconstruction. The  $\Upsilon$  acceptance is calculated by generating large samples of Monte Carlo  $\Upsilon \rightarrow \mu^+ \mu^-$  events using the full detector simulation with the  $p_T$  distributions of  $\Upsilon(1S)$ ,  $\Upsilon(2S)$  and  $\Upsilon(3S)$  states tuned to match the those observed in the data. Separate acceptance distributions are calculated for the background component, which is generated with  $p_T$ , rapidity and invariant mass distributions tuned to agree with the observed distributions in the background. The calculated acceptance includes the simulation of the measured trigger and event reconstruction efficiencies and is weighted to reproduce accurately the observed distribution of vertex positions along the beam axis.

We observe that the angular distributions of the background in the prompt and displaced samples are very similar. Figure 2 shows a comparison of the angular distributions observed in the prompt and displaced samples measured in the Collins-Soper frame and projected onto the  $\cos\theta$  and  $\varphi$  axes. We find this to be true for invariant mass below the  $\Upsilon(1S)$  and above the  $\Upsilon(3S)$  mass, so we infer that the displaced sample will provide an accurate description of the angular distribution of background in the mass regions that contain the  $\Upsilon(nS)$  signals. Thus, we describe the number of events in a given angular interval in the prompt and displaced samples by functions of the form

$$\frac{dN_p}{d\Omega} \sim \sigma_{\Upsilon} f_p \mathcal{A}_{\Upsilon}(\cos\theta, \varphi) \cdot w(\cos\theta, \varphi; \vec{\lambda}_{\Upsilon}) + \sigma_d s_p \mathcal{A}_{\text{bkg}}(\cos\theta, \varphi) \cdot w(\cos\theta, \varphi; \vec{\lambda}_{\text{bkg}}) \quad (3)$$

$$\frac{dN_d}{d\Omega} \sim \sigma_{\Upsilon} (1 - f_p) \mathcal{A}_{\Upsilon}(\cos\theta, \varphi) \cdot w(\cos\theta, \varphi; \vec{\lambda}_{\Upsilon}) + \sigma_d \mathcal{A}_{\text{bkg}}(\cos\theta, \varphi) \cdot w(\cos\theta, \varphi; \vec{\lambda}_{\text{bkg}}) \quad (4)$$

in which  $\sigma_{\Upsilon}$  and  $\sigma_d$  are the  $\Upsilon$  and displaced background event yields,  $f_p$  is the fraction of  $\Upsilon$  signal populating the prompt sample, and  $s_p$  is the ratio of background yields in the prompt and displaced samples. The angular distributions for signal and background are described by parameters  $\vec{\lambda}_{\Upsilon}$  and  $\vec{\lambda}_{\text{bkg}}$ . The angular distribution of the signal has the form of Equation 1 but an additional  $\cos^4\theta$  term is added to the background angular distribution function to facilitate its description in some ranges of  $p_T$  and invariant mass. The scale factor  $s_p$  is constrained by the previous fit performed to the displaced sample and the sidebands of the prompt sample.

Figure 3 shows the comparison of the projected angular distributions observed in the mass range  $9.25 < m(\mu^+ \mu^-) < 9.65 \text{ GeV}/c^2$ , which contains the  $\Upsilon(1S)$  signal, with the weighted acceptance distributions after maximizing the likelihood function. The analysis is performed in 8 ranges of  $p_T$  that range between 0 and 40  $\text{GeV}/c$  in mass ranges containing the three  $\Upsilon(nS)$  states as well as in the sidebands which contain only background. Figure 4 shows an example from the analysis in the S-channel helicity frame where the one-sigma contours for the  $\lambda_{\theta}$  and  $\lambda_{\varphi}$  parameters are plotted for all three  $\Upsilon(nS)$  states and for the background. This demonstrates the significant difference between the angular distributions of the signals and the background and illustrates that the angular distribution of the background changes significantly over the full range of invariant mass considered.

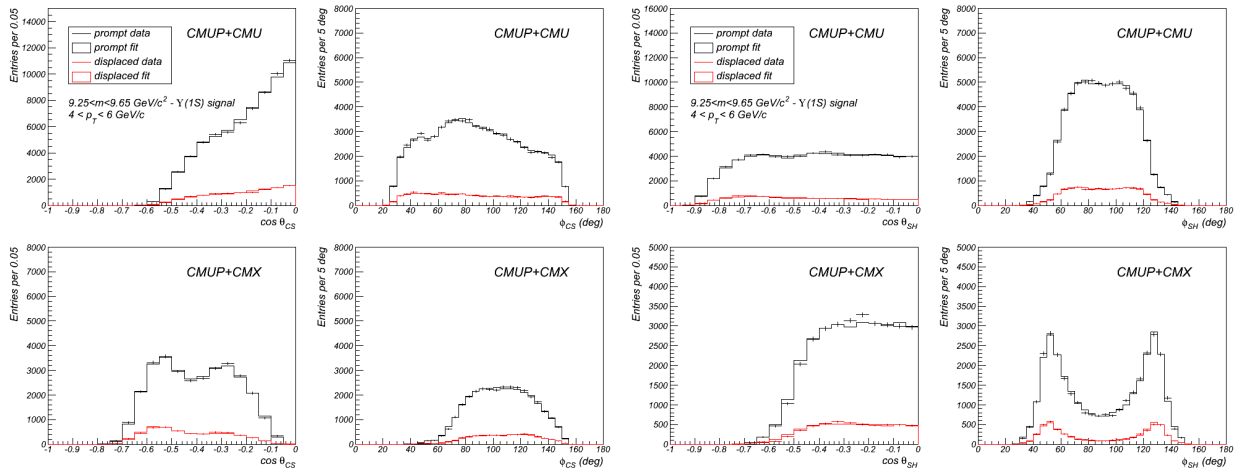
CDF Run II Preliminary,  $6.7 \text{ fb}^{-1}$ 

FIG. 3: Comparisons between angular distributions observed in the data (error bars) with the fit (histograms) for di-muon invariant masses in the region containing the  $\Upsilon(1S)$  signal. The prompt sample is indicated in black while the displaced sample is in red. The left plots show the angular distributions measured in the Collins-Soper frame and the right plots show them in the S-channel helicity frame.

The analysis is performed in both the Collins-Soper and S-channel helicity frames which allows us to calculate and compare the rotational invariant quantity  $\tilde{\lambda} = (\lambda_\theta + 3\lambda_\varphi)/(1 - \lambda_\varphi)$  in each reference frame. Figure 5 shows an example of the one-sigma confidence intervals on the parameters  $\lambda_\theta$  and  $\lambda_\varphi$  measured in both reference frames. Figure 6 shows the comparison as a function of  $p_T$  for the three  $\Upsilon(nS)$  states. Based on the results of toy Monte Carlo simulations, the difference between values of  $\tilde{\lambda}$  measured in each reference frame is consistent with deviations typical of purely statistical fluctuations.

Figures 7 to 9 show graphs of  $\lambda_\theta$ ,  $\lambda_\varphi$  and  $\lambda_{\theta\varphi}$  measured in both Collins-Soper and S-channel helicity frames for three  $\Upsilon(nS)$  states.

We evaluated the sizes of several sources of systematic uncertainty in the parameters  $\lambda_\theta$ ,  $\lambda_\varphi$  and  $\lambda_{\theta\varphi}$ . Alternate acceptance distributions were calculated with all trigger and muon selection efficiencies varied simultaneously by  $\pm 1 \sigma$ . The analysis was repeated using these acceptance distributions and the difference between parameters compared with those obtained using the nominal acceptance distributions is assessed as a systematic uncertainty. We also considered a quadratic function with which to parametrize the prompt scale factor as a function of invariant mass which changes slightly the calculated level of background in the prompt sample. Although differences between values of the rotational invariant  $\tilde{\lambda}$  in each reference frame is consistent with purely statistical variations in most cases, the lowest  $p_T$  ranges for the  $\Upsilon(3S)$  show systematic differences. In all cases, we use this difference to calculate the variation in  $\lambda_\theta$  and  $\lambda_\varphi$  due to the systematic uncertainty of the fit model applied in different reference frames, this is usually much smaller than the statistical uncertainties.

These results can be compared with previously published measurements of the parameter  $\lambda_\theta$  in the S-channel helicity frame. Figure 10 shows a comparison of the current result with a CDF analysis of Run I data[3]. The current result is consistent with the previous CDF measurement, but as shown in Figure 11, it is not consistent with the published Run II result from  $D\bar{O}$ . We estimate the statistical significance of the discrepancy to be approximately  $4.5\sigma$ .

## V. SUMMARY

We have analyzed the complete angular distribution of  $\Upsilon(nS) \rightarrow \mu^+\mu^-$  decays and find no evidence for strong polarization over a wide range of  $p_T$ . The measurement of  $\lambda_\theta$  for the  $\Upsilon(1S)$  state in the S-channel helicity frame can be compared with previously published measurements and is found to be in agreement with a Run I CDF analysis[3], but inconsistent with a Run II  $D\bar{O}$  measurement[4] at the level of about  $4.5 \sigma$ .

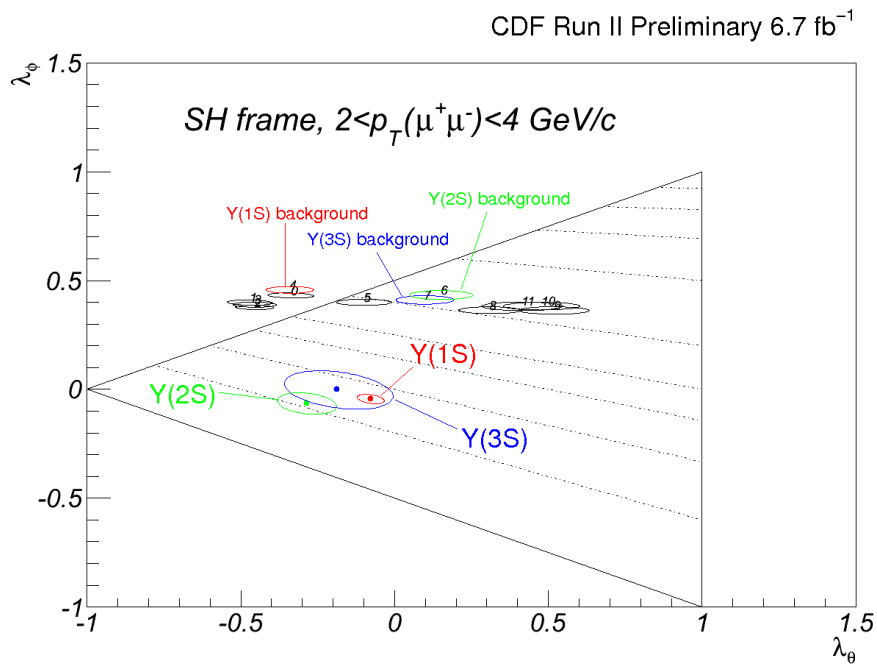


FIG. 4: One-sigma confidence regions for the  $\lambda_\theta$  and  $\lambda_\varphi$  parameters measured in the S-channel helicity frame both the  $\Upsilon(nS)$  signals and the ranges of di-muon invariant mass containing only background. The triangular region indicates the range of values allowed for the decay of a massive vector particle into two fermions.

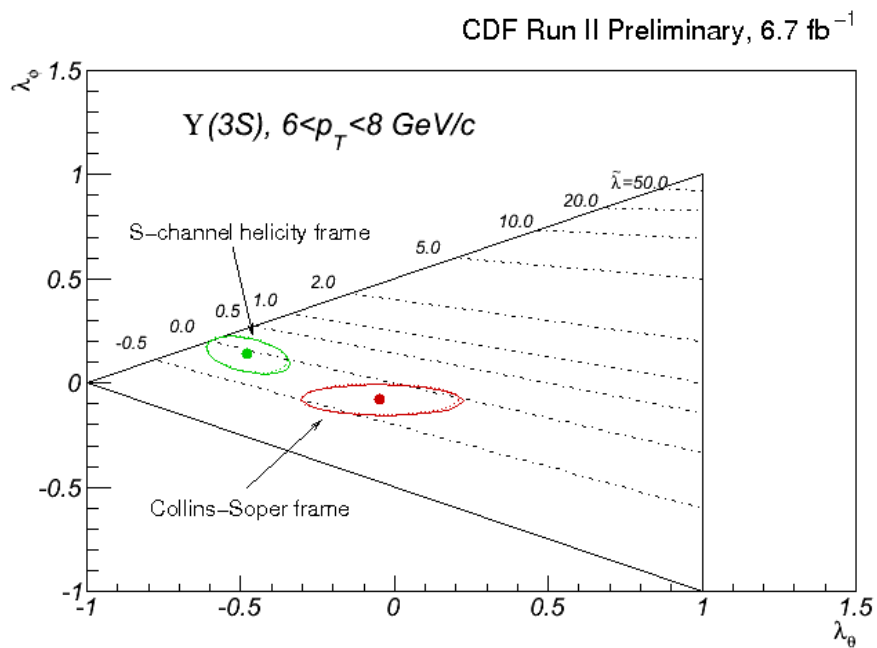


FIG. 5: One-sigma confidence intervals for  $\lambda_\theta$  and  $\lambda_\varphi$  for the  $\Upsilon(3S)$  state measured in the S-channel helicity frame (green) and the Collins-Soper frame (red). Dot-dashed lines indicate combinations of  $\lambda_\theta$  and  $\lambda_\varphi$  with equal  $\tilde{\lambda}$ . While the parameters measured in each reference frame are different, they both line close to the same lines of equal  $\tilde{\lambda}$ .

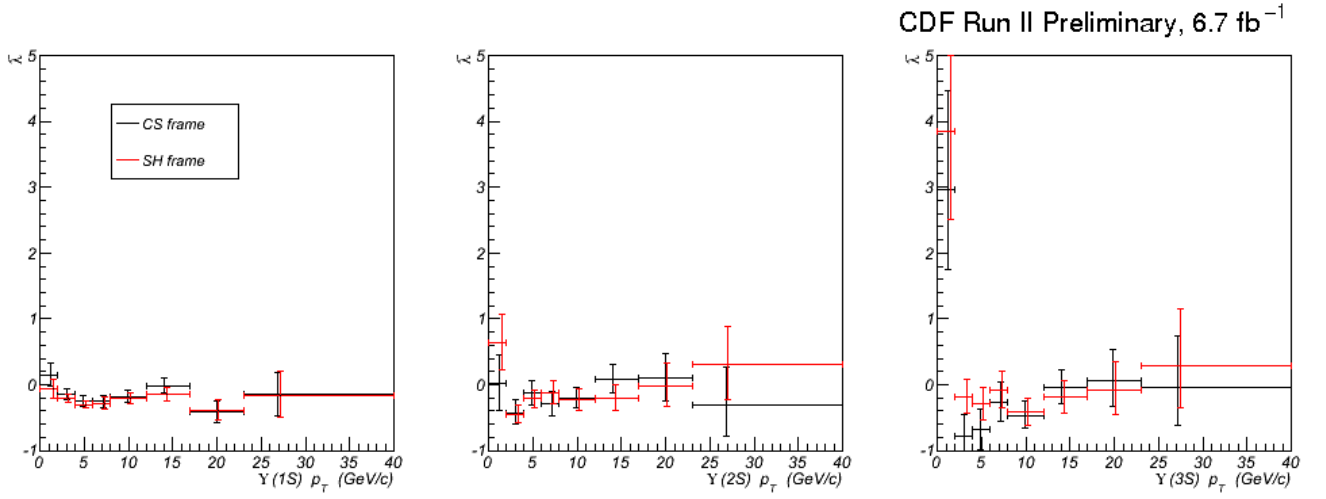


FIG. 6: Values of the rotational invariant quantity  $\tilde{\lambda} = (\lambda_\theta + 3\lambda_\varphi)/(1 - \lambda_\varphi)$  calculated in the Collins-Soper frame (black) and in the S-channel helicity frame (red) as a function of  $p_T(\Upsilon)$  for the  $\Upsilon(1S)$ ,  $\Upsilon(2S)$  and  $\Upsilon(3S)$  states. For a given  $p_T$  interval, the statistical errors on  $\tilde{\lambda}_{CS}$  and  $\tilde{\lambda}_{SH}$  are almost fully correlated.

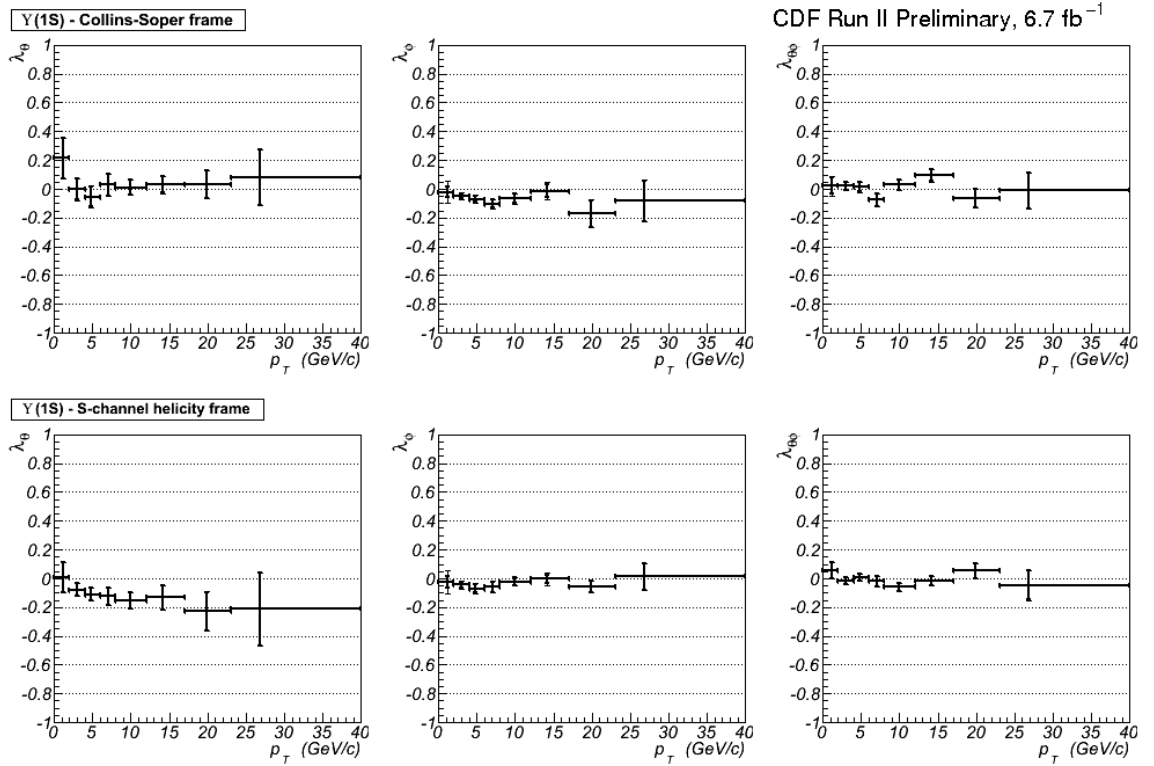


FIG. 7: Fitted parameters  $\lambda_\theta$ ,  $\lambda_\varphi$  and  $\lambda_{\theta\varphi}$  as a function of  $p_T$ , measured in the Collins-Soper frame (top row) and the S-channel helicity frame (bottom row) for the  $\Upsilon(1S)$ . Error bars include both statistical and systematic uncertainties.

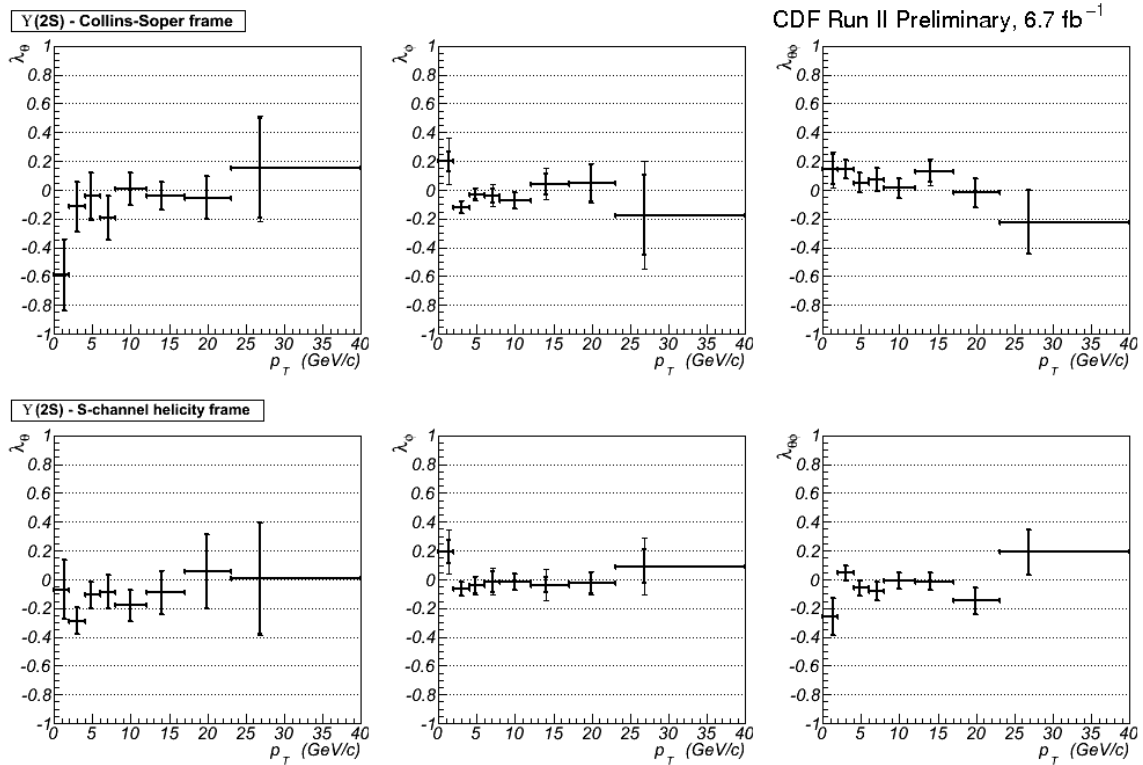


FIG. 8: Fitted parameters  $\lambda_\theta$ ,  $\lambda_\phi$  and  $\lambda_{\theta\phi}$  as a function of  $p_T$ , measured in the Collins-Soper frame (top row) and the S-channel helicity frame (bottom row) for the  $\Upsilon(2S)$ . Error bars indicate both statistical and systematic uncertainties.

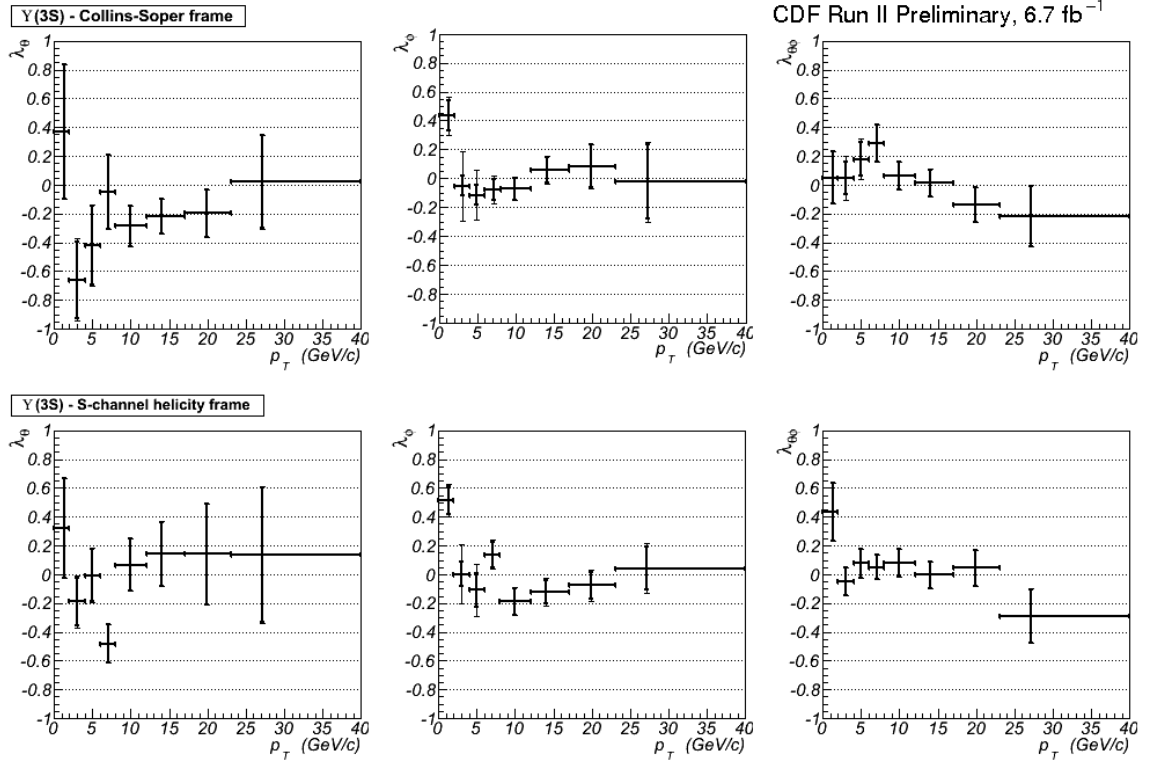


FIG. 9: Fitted parameters  $\lambda_\theta$ ,  $\lambda_\varphi$  and  $\lambda_{\theta\varphi}$  as a function of  $p_T$ , measured in the Collins-Soper frame (top row) and the S-channel helicity frame (bottom row) for the  $\Upsilon(3S)$ . Error bars indicate both statistical and systematic uncertainties.

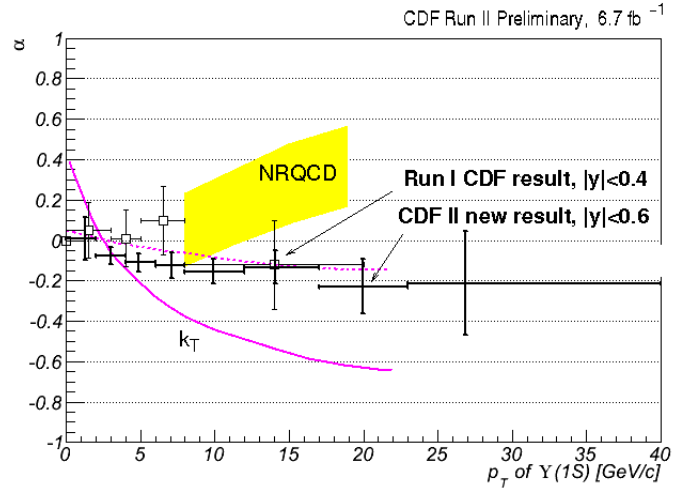


FIG. 10: Comparison of the parameter  $\alpha \equiv \lambda_\theta$  for  $\Upsilon(1S)$  decays measured in the S-channel helicity frame as a function of  $p_T$  with the previously published CDF result[3]. Although the ranges of  $|y|$  differ, we do not observe the angular distribution to change rapidly with  $|y|$ , at least in the central region of rapidity. The yellow band indicates the range of values suggested by NRQCD[1] while the magenta curves show predictions of the  $k_T$  factorization model[2] for two extreme sets of parameters.

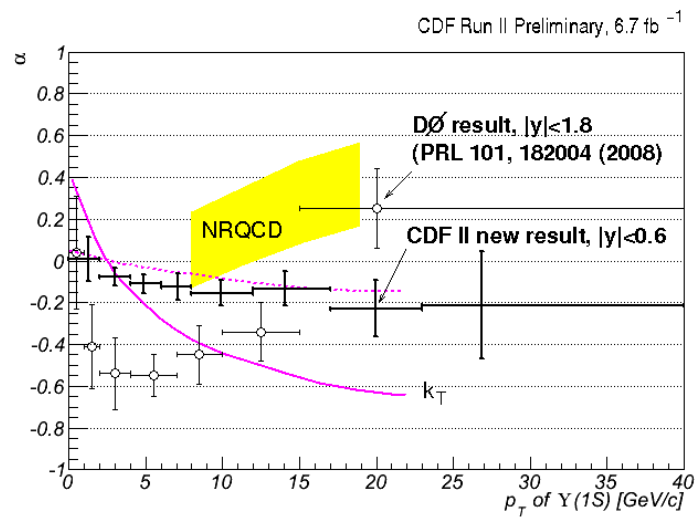


FIG. 11: Comparison of the parameter  $\alpha \equiv \lambda_\theta$  for  $\Upsilon(1S)$  decays, measured in the S-channel helicity frame as a function of  $p_T$ , with the previously published DØ result[4].

We thank the Fermilab staff and the technical staffs of the participating institutions for their vital contributions. This work was supported by the U.S. Department of Energy and National Science Foundation; the Italian Istituto Nazionale di Fisica Nucleare; the Ministry of Education, Culture, Sports, Science and Technology of Japan; the Natural Sciences and Engineering Research Council of Canada; the National Science Council of the Republic of China; the Swiss National Science Foundation; the A.P. Sloan Foundation; the Bundesministerium für Bildung und Forschung, Germany; the Korean World Class University Program, the National Research Foundation of Korea; the Science and Technology Facilities Council and the Royal Society, UK; the Institut National de Physique Nucleaire et Physique des Particules/CNRS; the Russian Foundation for Basic Research; the Ministerio de Ciencia e Innovación, and Programa Consolider-Ingenio 2010, Spain; the Slovak R&D Agency; the Academy of Finland; and the Australian Research Council (ARC).

- 
- [1] E. Braaten and J. Lee, Phys. Rev. D **63**, 071501(R); P. Cho and A.K. Leibovich, Phys. Rev. D **53**, 150 (1996); **53**, 6203 (1996).
  - [2] S.P. Baranov and N.P. Zotov, JETP Lett. 86, 435 (2007).
  - [3] D. Acosta, *et al.* (CDF Collab.), Phys. Rev. Lett. 88, 161802 (2002).
  - [4] V.M. Abazov, *et al.* (DØ Collab.), Phys. Rev. Lett. 101, 182004 (2008).
  - [5] F. Abe, *et al.*, Nucl. Instrum. Methods Phys. Res. A **271**, 387 (1988); D. Amidei, *et al.*, Nucl. Instrum. Methods Phys. Res. A **350**, 73 (1994); F. Abe, *et al.*, Phys. Rev. D **52**, 4784 (1995); P. Azzi, *et al.*, Nucl. Instrum. Methods Phys. Res. A **360**, 137 (1995); The CDFII Detector Technical Design Report, Fermilab-Pub-96/390-E
  - [6] T. Aaltonen, *et al.* (CDF Collab.), arXiv:1107.2304v2 [hep-ex], Fermilab-Pub-11-315-E, accepted by PRL.